JMEPEG (2021) 30:4808–4818
https://doi.org/10.1007/s11665-021-05919-6

1059-9495/$19.00

Defects in Metal Additive Manufacturing Processes

M.C. Brennan, J.S. Keist, and T.A. Palmer

The formation of defects within additive-manufactured (AM) components is a major concern for critical structural and cyclic load applications. Thus, understanding the mechanisms of defect formation in fusion-based processes is important for prescribing the appropriate process parameters specific to the alloy system and selected processing technique. This article discusses the formation of defects within metal additive manufacturing, namely fusion-based processes and solid-state/sintering processes. Defects observed in fusion-based processes include lack of fusion, keyhole collapse, gas porosity, solidification cracking, solid-state cracking, and surface-connected porosity. The types of defects in solid-state/sintering processes are sintering porosity and improper binder burnout. The article also discusses defect-mitigation strategies, such as postprocess machining, surface treatment, and postprocessing HIP, to eliminate defects detrimental to properties from the as-built condition. The use of noncontact thermal, optical, and ultrasound techniques for inspecting AM components are also considered. The final section summarizes the knowledge gap in our understanding of the defects observed within AM components.

Keywords additive manufacturing, hot isostatic pressing, machining, manufacturing defects, surface treatment

1. Types of Defects in Fusion-Based Processes

The formation of defects within additive-manufactured (AM) components is a major concern for critical structural and cyclic load applications. If not removed, the presence of defects within an AM component can have a detrimental impact on its performance during service. Thus, understanding the mechanisms of defect formation in fusion-based processes is important for prescribing the appropriate process parameters specific to the alloy system and selected processing technique.

Metal AM processes are largely split between two main processes: powder-bed fusion (PBF) processes and directed-energy deposition (DED). In PBF processes, a thin layer of powder is evenly distributed across a build platform while a focused energy source, such as a laser or electron beam, selectively fuses powder to a metal substrate to produce net shape components with high levels of geometric complexity. The DED processes use powder flow controlled by an inert gas through a set of nozzles and a focused laser or electron beam to produce large, near-net shape structures. Processing conditions for AM can be significantly different between PBF and DED, as well as between various AM processing chambers. Rapid heating, cooling, and solidification inherent in the fabrication of AM metal components results in complex microstructures and properties that may significantly differ from those typically observed in wrought or cast components.

Additive manufacturing shares important physical processing attributes to welding, such as a moving heat source, which forms a fusion zone with recirculating liquid metal (Ref 1). The complicated transient conditions inherent of AM processing impact the resulting metallurgical quality, microstructures, residual stresses, and distortions observed within the components (Ref 1). Instabilities during processing often lead to the formation of internal defects. Defects observed within AM components typically fall within two main categories: porosity and cracks. Defects can also result from the entrapment of impurities within the component during AM processing. These defects can reduce the mechanical properties of the component (Ref 1, 2) and can significantly reduce its cyclic fatigue performance (Ref 3, 4). While AM lacks robustness, identifying the location, size, shape, and volume of the defects formed, followed by healing any porosity through postprocessing hot isostatic pressing (HIP), leads to the restoration of mechanical strength in the AM components.

1.1 Lack of Fusion

Lack of fusion encompasses defects that are irregular, elongated shapes ranging from 50 μm to several millimeters in size, as shown in Fig. 1. In this instance, the Ti-6Al-4V component was processed using DED, which more often leads to the millimeter-sized defects. In some cases, unmelted powder particles are present within the lack-of-fusion region due to the evolution of the melt pool during processing. Lack-of-fusion defects are a result of insufficient overlap between passes, influenced by a mismatch in hatch-spacing parameters (Ref 5, 6), where *hatch spacing* refers to the distance between two adjacent passes (Ref 2, 7). Lack-of-fusion defects have been intentionally formed in build layers for multiple metal alloys by manipulating process parameters that would typically produce a component with minimum defects (Ref 7-10). Selection of larger hatch-spacing parameters has demonstrated a reduction in overlap between two neighboring passes, leading to a higher probability of lack of fusion. Decreased hatch spacing corre-

M.C. Brennan, J.S. Keist, and **T.A. Palmer**, The Pennsylvania State University, University Park, PA, USA. Contact e-mails: mxb1033@psu.edu, jsk25@psu.edu, and tap103@psu.edu.

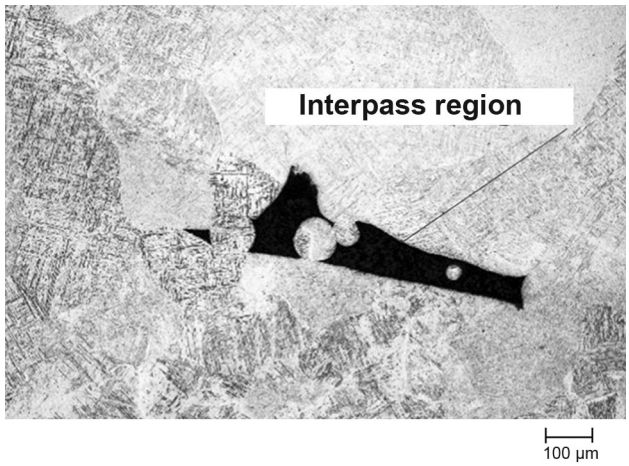

Fig. 1 Lack-of-fusion defect formed in a directed-energy-deposition-processed Ti-6Al-4V component

sponded to larger regions of overlap and sufficient fusion between passes (Ref 1, 11).

The energy source and the processing parameters (i.e., travel speed, spot size, standoff, and power) to fuse molten metal ultimately dictate the mechanisms of defect formation in components. Parameter selection requires a significant understanding of the evolution of the temperature field during the deposition process, which is built on a quantitative assessment of the absorption of heat energy by the feedstock material. In particular, for DED processes, a fraction of the total heat is spent to heat the powder particles as they emerge from the nozzle and travel through the beam (Ref 1). The heat absorbed by the powder particles is dependent on several factors, including their density, thermophysical properties, shape, size distribution, free-flight duration through the beam, and gas velocity (Ref 12). Powder particles, although heated to a high temperature, do not always reach their melting temperature. Nonetheless, the excess energy impinges on the build surface and forms a molten pool. The absorption energy depends on beam characteristics, deposit geometry, and shielding gas. For a laser-assisted DED process with argon shielding gas, the absorption coefficient for a laser beam with a 1064 nm wavelength remains between 0.3 and 0.7, depending on its solid-liquid state (Ref 12).

Because of the rapid heating, melting, and solidification introduced by the moving heat source, regions of the build experience repeated heating and cooling, which affects its local structure and properties (Ref 1). While welding is more comparable to the additive process than casting, there are significant differences involved with how the heat source interacts with a stream of powder versus a solid metal. Heat source interaction with the feedstock creates a progressive buildup as more material is added, thus creating a history of thermal cycles and transient change in geometry of the AM component. Parameter selection of the AM process ultimately influences the bead size and geometry for each metal alloy system.

1.2 Keyhole Collapse

Keyhole porosity is observed in high-energy-density welding processes (Ref 13, 14) and has been linked to macroporosity in laser and laser-arc hybrid welds (Ref 13, 15-17). Without careful control of keyhole-mode melting, keyholes can become unstable and repeatedly form and collapse, leaving voids inside the deposit that consist of entrapped vapor (Ref 18). The root of keyhole porosity is initiated by the generation of a deep V-shaped melt pool and vaporizing elements within the pool (Ref 5). Keyhole porosity for the PBF process is the result of a rapid, local melting of powder by a continuous laser heat source. Stages of keyhole formation may be illustrated by the dynamic x-ray images captured in Fig. 2. The impingement on the build surface induces an oscillation behavior that effectively spreads the molten pool across the surface. In some cases, instability in the molten pools leads to material ejection and results in a pore forming at the bottom of the pool. This pore is then trapped and solidified beneath the surface (Ref 19). Keyhole pores vary in shape and range in size from 10 to 50 μm. Pores that are not surface connected can be healed by postprocessing HIP.

1.3 Gas Porosity

Gas-entrapped pores are characterized by their spherical shape, as indicated in Fig. 3. These defects are typically on the order of 5 to 20 μm when processed through PBF (Ref 10), while parts produced with DED are characteristically larger in size (>50 μm) (Fig. 3). Pores form and evolve over time through gas entrapment, supersaturation of dissolved gases, and chemical reactions that produce gaseous species within the molten pool (Ref 1, 2, 20). A higher likelihood of nucleating entrapped gas pores is apparent when the equilibrium pressure of a gas exceeds the combined hydrostatic, atmospheric, and capillary pressure. Nucleated pores lead to vacancies, where supersaturated gases within a molten pool can diffuse (Ref 21). When rapid cooling takes place, pore nucleation sites are likely to become trapped in the molten pool. However, slower cooling and solidification rates allow these pores to grow and sometimes coalesce with neighboring pores. Once pores reach a critical size, they separate from the solidification front and float to the surface of the solidifying pool (Ref 20). Previous investigations demonstrated that high solidification rates and high gas content increased pore concentrations in metal alloys (Ref 21). Furthermore, retained gas concentrations within each bubble contribute to pore growth based on the imbalance in mass transfer between two fluids present in the Marangoni flow (Ref 22).

1.4 Solidification Cracking

Solidification cracking present in weld metals is a complex phenomenon occurring in the fusion zone near the end of solidification. Solidification cracking, or hot cracking, is driven by a temperature gradient and initiated by the interaction between metallurgical and mechanical factors (Ref 23). Solidification microstructures are controlled by thermal-metallurgical interactions, such as phase transformations, whereas local stress and strain behaviors are controlled by thermal-mechanical interactions. For solidification cracking to occur, the combination of mechanical restraint (strain) and susceptible microstructure must be present (Ref 4). Thermal-metallurgical factors contributing to solidification cracking in welding practices and applicable for AM fusion-based processes are outlined in Fig. 4, while thermal-mechanical factors are indicated in Fig. 5.

For certain alloy systems, cracks can form during the terminal solidification stages. These cracks initiate upon an accumulation of shrinkage strains along grain boundaries and interdendritic regions where a liquid film is distributed (Ref 4).

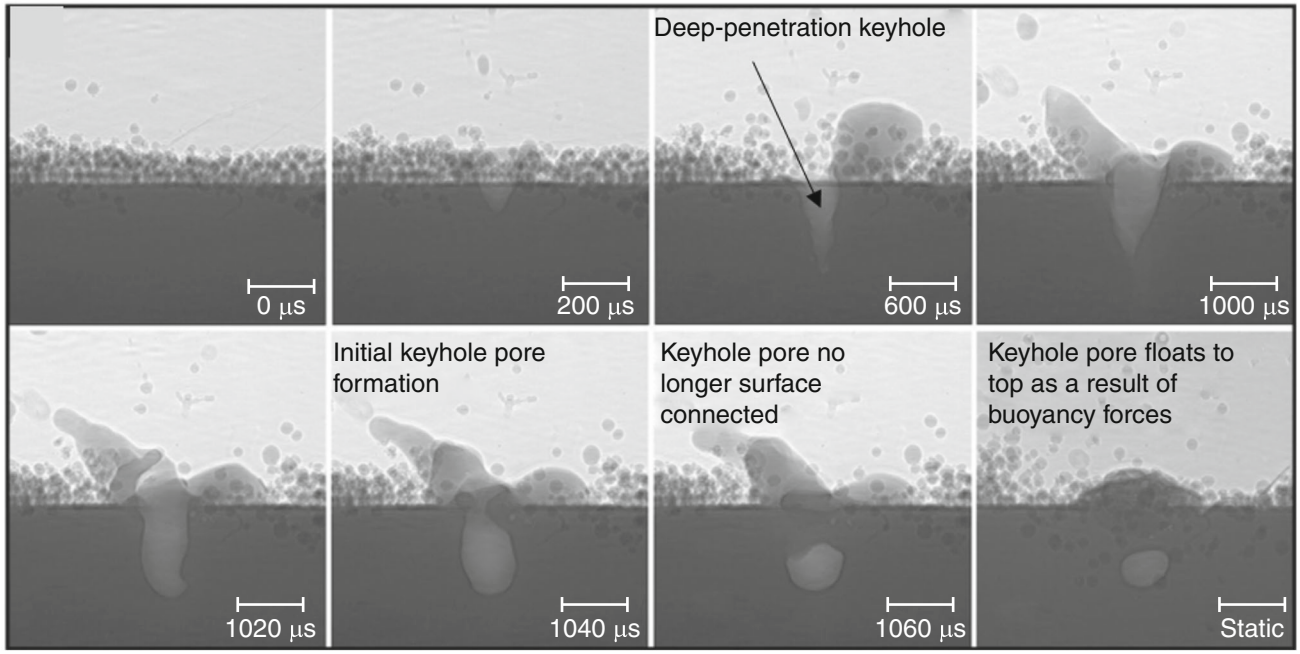

Fig. 2 Dynamic x-ray images of a laser powder-bed fusion process for Ti-6Al-4V, where a keyhole pore is formed upon increasing the laser power used for processing. Scale bars are 200 μm. Source: Ref 19

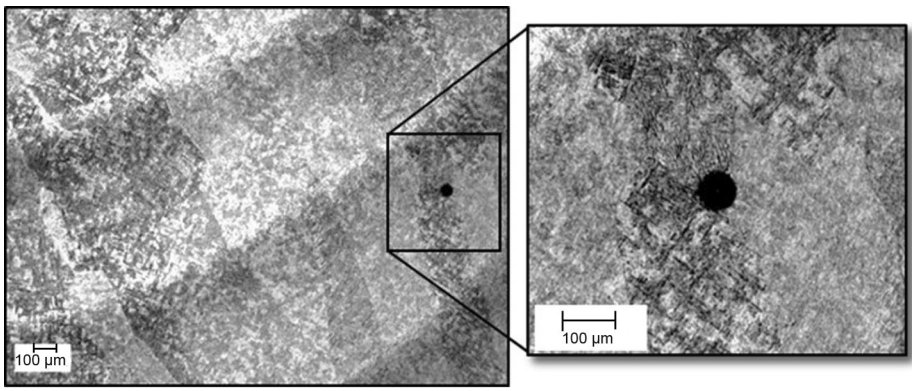

Fig. 3 Entrapped gas porosity located in a directed-energy deposition Ti-6Al-4V component

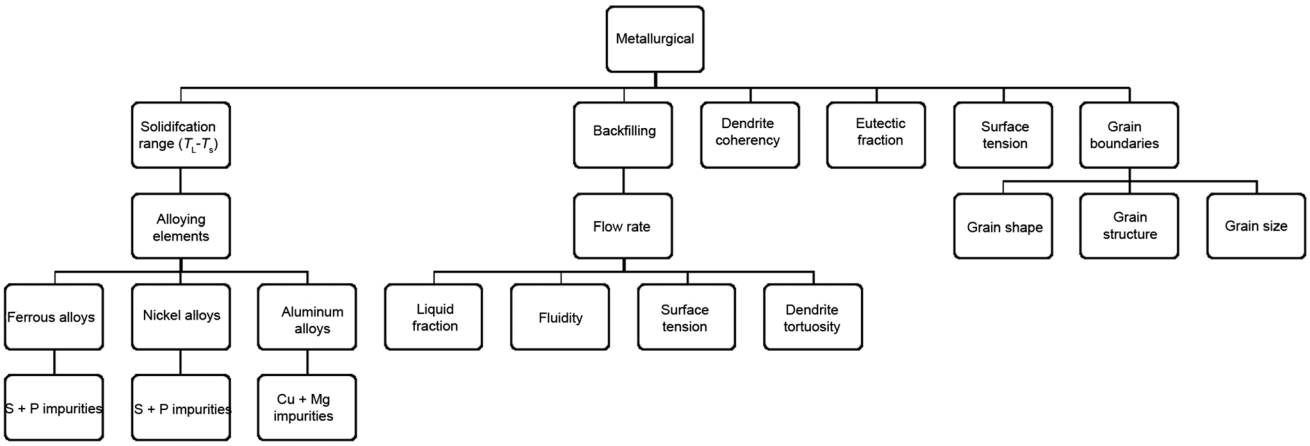

Fig. 4 Thermal-metallurgical interactions influencing the susceptibility of solidification cracking

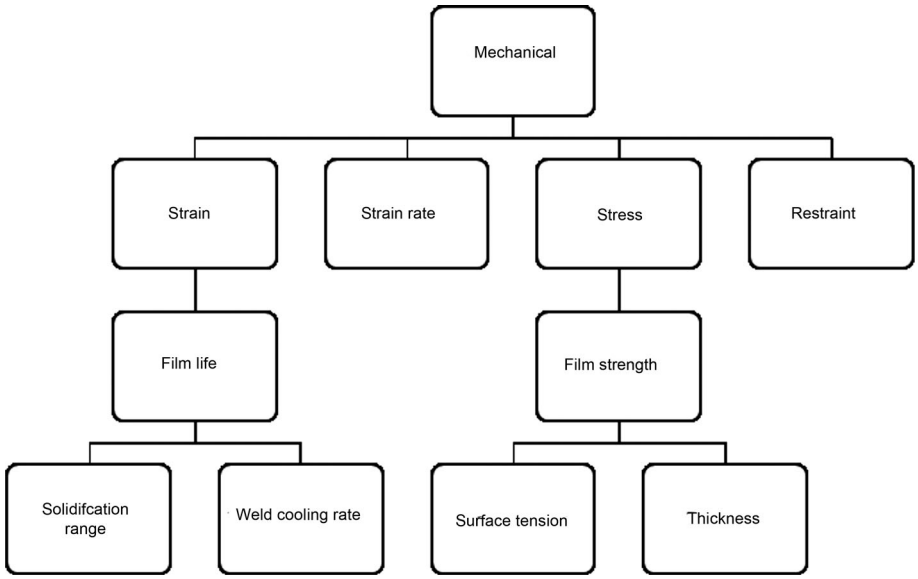

Fig. 5 Thermal-mechanical interactions influencing the susceptibility of solidification cracking

Primary material factors include the solidification temperature range, also referred to as the brittle temperature range, and the interfacial liquid morphology at terminal solidification stages. Alloys with a wide solidification temperature range are more susceptible to solidification cracking than alloys that solidify over a narrow temperature range, due to the accumulated thermal strain proportionality to the temperature range. Wide solidification temperature ranges are often consequences of compositional variations that contribute to lower eutectics. An alloy with a wide solidification temperature range may also exhibit a less coherent dendritic structure during solidification that allows for the formation of shrinkage cracks due to the lack of liquid backfilling (Ref 4).

Backfilling, or the drawing of liquid through a dendritic network to feed solidification shrinkage, can often avoid hot tearing during solidification and is controlled by dendrite tortuosity, liquid fraction, fluidity, and surface tension. The backfilling potential increases when surface tension is low and when the last liquid to solidify can wet the dendrites. A higher backfilling potential means that there is a higher probability that a continuous liquid network will be present during solidification to provide backfilling. In cases where no wetting occurs between the dendrites, globules can act as a bridge between solidifying dendrites to resist the effects of increases in strain and thus avoid cracking (Ref 23, 24). It is in the systems that exhibit intermediate values of wettability and backfilling potential where cracking can occur during solidification. For example, in niobium superalloys the terminal liquid between 1 and 10 vol% exhibits low surface tension, which interferes with the solid-solid bridges; this system does not exhibit enough backfilling potential to compensate for shrinkage (Ref 24).

A mechanical factor, such as strain, can accumulate during soldification and initiate cracking. In the strain model proposed by Pellini (Ref 25), cracking can occur when the intergranular liquid film is strained above a critical value. The amount of strain that the liquid film will experience is dependent on the solidification range and the cooling rate. Cracking occurs when the deformation curve, represented by the strain across the brittle temperature range in Fig. 6, intersects the ductility curve for the alloy system, which is defined as the critical strain value

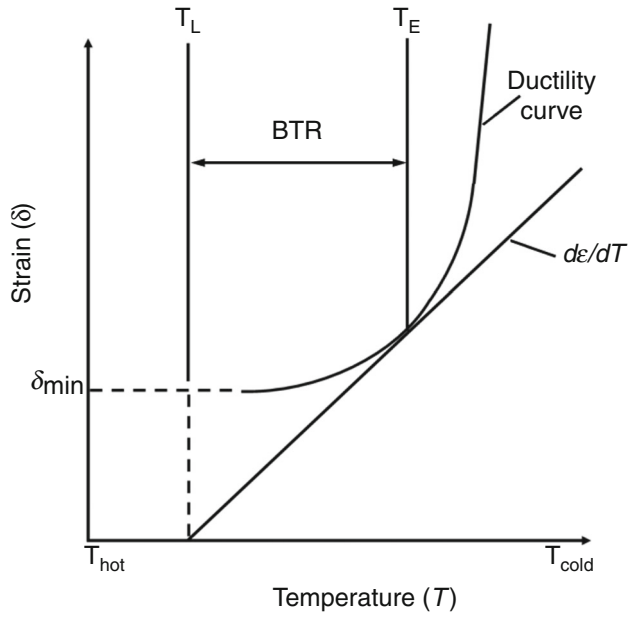

Fig. 6 Schematic of the ductility curve, brittle temperature range (BTR), and strain as a function of temperature ($d\varepsilon/dT$). Cracking occurs when the strain across the BTR ($d\varepsilon/dT$) intersects the ductility curve. Source: Ref 26

(Ref 26). The critical strain value of the liquid film is dependent on both surface tension and film thickness, where strength is decreased under significant restraints.

1.5 Solid-State Cracking

Solid-state cracking originates from continuous heating and cooling of various weldable metals and is identified as one of five types:

- Ductility-dip cracking (DDC)
- Reheat and postweld heat treatment (PWHT) cracking
- Strain age cracking (SAC)

- Lamellar cracking (delamination)
- Copper contamination cracking (CCC) (Ref 4)

The deviation between each type of solid-state cracking is differentiated by the mechanisms and the preferred location where the cracks form.

Ductility-dip cracking occurs upon a sharp reduction in ductility for copper, aluminum, nickel, titanium, and austenitic stainless steel alloys at temperatures between T_s and $0.5T_s$ (Ref 4). This reduction in ductility may be predicted based on the knowledge of the solidification range and minimum strain induced. While impurities are not always ideal for processing materials, impurity segregation does not suggest any detrimental impacts, because the boundary liquidation does not play a role for this type of solid-state cracking. In fact, DDC always occurs intergranularly along the migrated grain boundaries. While the mechanisms influencing DDC have been widely debated, the factors that influence DDC in fused metals include high-angle grain boundaries, temperature, composition, restraint, and precipitates that form along grain boundaries at the solid state and concentrate at the triple point (Ref 4).

In contrast, reheat cracking is associated with PWHT and stress-relief treatments that are typically used to temper martensitic structures and reduce residual stresses. While reheat cracking may not be immediately present in an as-built AM structure, any postprocessing heat treatment may subject the parts to such condition. Low-alloy steels typically experience this type of cracking due to their secondary carbide formers (chromium, molybdenum, vanadium) contained within the melt. Additionally, materials that experience strong precipitation reactions are susceptible to this type of solid-state cracking. Reheat cracking may be prevented by controlling composition, weld conditions, residual stresses, stress relaxation, stress concentrations, or by "buttering" the substrate used as the base plate for joining (Ref 4).

On the other hand, SAC occurs intergranularly in the heat-affected zone (HAZ) of precipitation-strengthened nickel-base alloys. The simultaneous local strain and aging conditions applied to the weld metal initiate the formation of this defect. Inconel 718, a precipitation-hardened nickel alloy popular for AM repair application, is resistant to SAC due to the reduced titanium and aluminum composition that contributes to a slower γ' precipitation rate. Materials with high minimum ductility are most susceptible to SAC.

The latter two solid-state cracking identities mentioned, lamellar cracking and CCC, have yet to be extensively explored in AM processes. However, both cracks are observed in the HAZ and have revealed detrimental effects on mechanical properties. Lamellar cracking dominantly occurs in plain carbon or low-alloy steels when sulfur and oxygen are trapped in the solidifying material and bond with other alloys, contributing to intermetallic impurities. By contrast, CCC is a consequence of liquid metal embrittlement observed in steels and cobalt-base alloys.

1.6 Impurities

In some cases, impurities can enhance mechanical behavior, strength, and ductility; however, in other instances they have led to reduced corrosion resistance and porosity in as-deposited structures. Powder-fed DED, wire-fed DED, and PBF additive manufacturing processes are all capable of producing defects contributed by impurities. Impurities are most often present in alloy chemistries of a material due to excess insoluble elements, such as carbon, oxygen, nitrogen, hydrogen, and chlorine (Ref 27). Impurities such as oxygen are likely to form oxides with alloying elements and contaminate virgin (pure) material feedstocks desirable for processing, if exposed to harmful environments prior to or during processing. Powder AM is likely to experience higher degrees of pores produced by impurities, due to the large surface area feedstock which increases the probability of being exposed to contamination. Furthermore, lower energy inputs that lead to smaller grains and more grain boundaries are likely to experience more regions for impurity nucleation along the grain boundaries and consequently diminished corrosion resistance.

Powder handling, feedstock production, and processing environments should be controlled following the necessary standards for chemistry control. Processing within an inert environment or using shielding gas such as argon during processing reduces the chances of possible contamination from impurities.

1.7 Surface-Connected Porosity

Surface-connected porosity can represent both a design feature, comparable to a scaffold used for AM bone structures, as well as a defect from previous vapors that resurfaced as bubbles but solidified prior to closing the pore shape during material transport. Surface porosity is considered invaluable for applications that desire strong bonds for other materials to grow, such as those used for medical implants (Ref 28). However, undesirable surface-connected porosity that cannot be removed by postprocess HIP results in poor surface roughness and diminished mechanical behavior (Ref 29, 30). An example of surface-connected porosity is shown in Fig. 7, a micrograph of a DED-processed 17-4PH stainless steel. Indications of lack of fusion and gas-entrapped pores are also identified in this 17-4PH AM component.

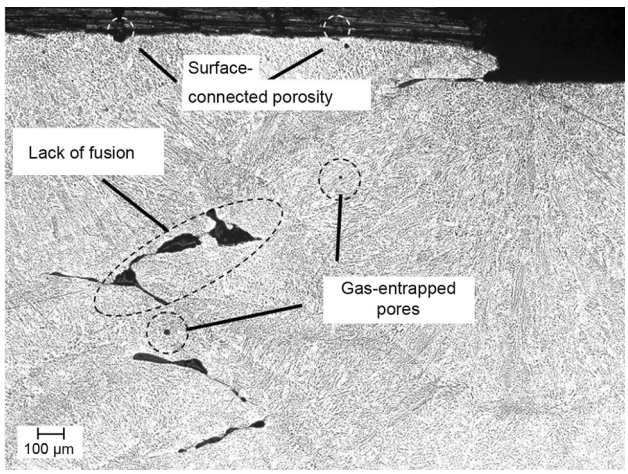

Fig. 7 Directed-energy-deposition-processed 17-4PH stainless steel indicating instances of lack of fusion, gas-entrapped pores, and surface-conducted porosity

2. Types of Defects in Solid-State/Sintering Processes

2.1 Sintering Porosity

Sintering is a well-established thermal process that transforms metallic or ceramic powders into bulk materials with improved mechanical strength, although in most cases, residual porosity results. The steps of solid-state sintering consist of solid-state atomic diffusion, recrystallization, and grain growth, while six different mechanisms are involved with mass transfer, including surface diffusion, evaporation condensation, grain-boundary diffusion, lattice diffusion, viscous flow, and plastic flow (Ref 31). The primary means of sintering is to achieve maximum density and strength based on the metallurgical bonds formed between neighboring particles. The bridge formed between metallurgically bonded particles is called a neck (Fig. 8).

Pores begin to take shape in the intermediate and final sintering stages. Initially, pores form interconnected channels along three grain edges (Fig. 9). As the sintering process progresses, the pore channels disconnect, and isolated pores form upon the dihedral angles exceeding 60° and nonuniform shrinkage. Coble proposed the two geometric models illustrated in Fig. 9—the channel pore model and the isolated pore model—to describe pore morphology evolution (Ref 32, 33). The closed pore encompassed between the particles is dependent on the number of neighboring particles.

In selective laser sintering, a laser beam irradiates each layer of powder that has been spread evenly on the previous layer and fuses the powder particles together to a high density ($>90\%$) to form the component. The resulting temperature gradient results in faster grain coalescence at the surface than the subsurface layers. Therefore, gas bubbles a few hundred micrometers in size are trapped in the melt layer due to their large size and fast solidification time. Several models have been developed based on mass transport and fluid dynamics to predict bubble dynamics and the resulting residual porosity. Reducing the particle size increases the rate at which sintering and densification occur (Ref 34). Choosing fast-diffusing alloying elements or shielding gases within a metal alloy matrix can also increase sintered component densification (Ref 34).

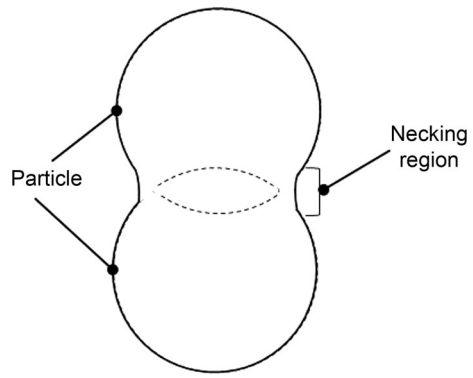

Fig. 8 Schematic representation of two particles that have been sintered and began to form a necking region

2.2 Improper Binder Burnout

Binder removal is one of the most critical steps in the powder metal industry. Defects can be produced by inadequate debinding, such as bloating, blistering, surface cracking, and large internal voids. Binder burnout depends on the internal structure of the green body and has the tendency to lead to structural change, where kinetics dictate the removal process. Binder distribution is dominated by capillary forces that depend on the physical properties of the molten binder and the rate of volatile product removal. Common techniques used for binder burnout include thermal, solvent, and catalytic. Generally speaking, thermal debinding is an inefficient process due to the excess production of vapor pressure in cores of molded parts, influenced by the elevated temperatures of the process contributing to the formation of defects. Alternatively, solvent techniques keep temperatures low to minimize defects, distortions, and debinding time. Burnout kinetics may be improved by modifying the binder to one with a higher melting point; however, vapor-phase transport, liquid diffusivity, and saturation solubility should also be recognized.

A transient diffusion and critical heating equation was developed for degradable products in an effort to achieve parts without defects (Ref 35). Some studies have accounted for interactions between the binder removal, density gradient, and resulting dimensional tolerances (Ref 36). Binder-removal kinetics showed heightened behavior when porosity was developed. The entire binder-removal process is dominated by two competitive processes: migration and vaporization. At certain zones of the removal process, low-density liquid phases become discontinuous, and molten binder/air interfaces intrude. In other instances, the binder vaporizes and diffuses through intraagglomerate pores into the surrounding air in the low-density zone, while capillary pressure differences continue to draw the binder into the high-density zones.

The most critical part of binder removal is the burnout of the low-molecular-weight components in the lower-temperature regime. The initial stages consist of low concentrations of pores that present challenges to the powder compacts and can lead to significant damage. The criterion for a failed burnout process is that the vapor pressure of the degradation product within the sample rises above 101 kPa (1 atm), and bubble nucleation and growth ensue. Pores for this process originate from the surface of the compact and spread to the interior of the structure during debinding (Fig. 10, step 1). Diffusion of a binder to an inner pore/binder interface precedes binder evaporation. Gases transport through the pores to the compact surface and are flushed away by a stream of nitrogen processing gas (Ref 37).

3. Defect-Mitigation Strategies

Defects present in AM metal components processed by PBF and DED demonstrate degrading mechanical and fatigue properties if the defects have not been removed. While for some applications excess postprocessing is not required, critical applications require extensive postprocess machining, surface treatment, and postprocessing HIP to eliminate defects detrimental to properties from the as-built condition. Another means of compensating for defect formation is to design builds accordingly to limit the susceptibility of forming defects in AM parts.

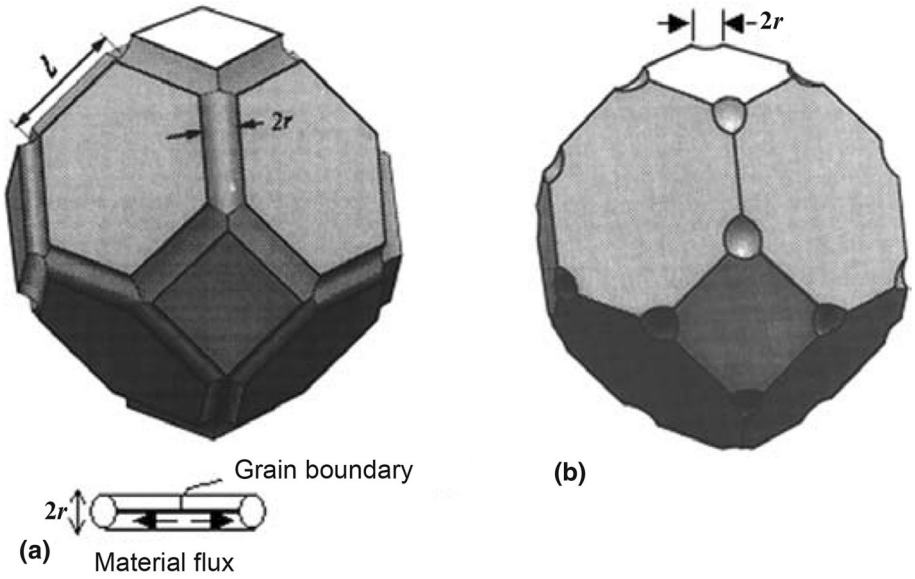

Fig. 9 Coble's geometrical models for (a) intermediate-stage and (b) final-stage sintering. Source: Ref 31

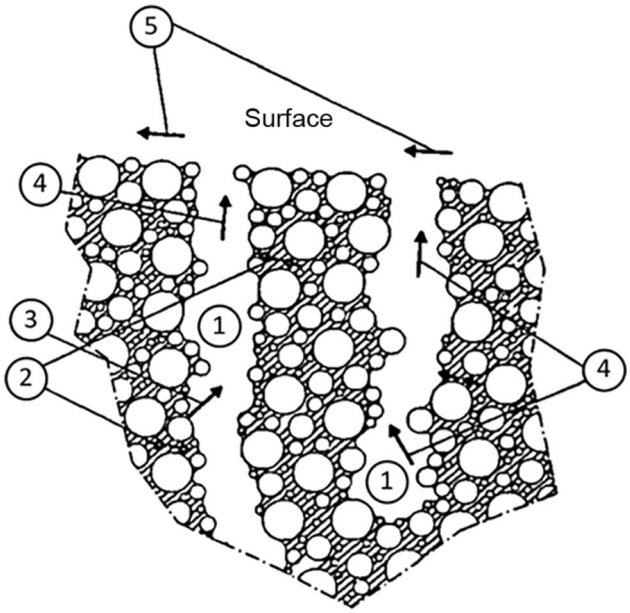

Fig. 10 Schematic of pore structure in a metal compact and pore-removal steps. (1) Pore formation during debinding. (2) Binder diffusion into inner pore/binder interface followed by (3) binder evaporation and (4) gaseous escape to the surface. (5) Nitrogen gas stream sweeps away any gaseous species that surface. Source: Ref 37

3.1 Postprocess Machining/Surface Treatment

Postprocess machining is desirable to remove any detrimental features such as surface-connected porosity, excess surface roughness caused by unmelted powder or individual traces from the laser, and removal of residual stresses as well as any oxidation or other impurities that have formed on the deposition surface. Alternatively, surface treatments are used to achieve a protective coating, corrosion resistance, and/or strength that may have been eliminated or modified during the postprocess machining. Postprocessing techniques include vibratory bowl abrasion, hot cutter machining, optical or hand polishing, milling, grinding, micromachine processing, chemical postprocessing, and electroplating (Ref 38).

Most often, postprocess machining in AM begins with the removal of support material and, in many cases, removal of the component from the substrate used to fuse the deposition. In some cases, support material may be removed with a pressurized gas nozzle or flushed with a soluble liquid, while in other instances, tooling such as abrasive saws or laser micromachining systems are required to remove excess material. Following support removal, AM deposits typically require some modification to as-built surfaces by using milling or grinding tools specific to the metal alloy. Some materials, particularly titanium alloys, are considered more difficult to machine. Titanium alloys are difficult to machine due to their low thermal conductivity and high chemical reactivity with most cutting tools. These properties often contribute to reduced tool life and poor surface finish (Ref 39).

Surface finishes of AM components are dictated by the application. In most PBF-processed parts, as-built surfaces distant from critical features are permissible for certain applications that do not experience excessive friction. Design tolerances are implemented to account for surface areas that require the surface of the part to be machined or refinished. In general, no standard machining or surface treatment procedures for AM metal have been developed; rather, they are material and application dependent.

3.2 Postprocess HIP

Postprocess HIP has been a long-established technique used to densify and consolidate powders as well as cast, sintered, and now AM products, based on the properties of heat transfer and phase transformations that occur during heat treatment. The HIP process applies a high-isostatic-pressure (100 to 200 MPa, or 15 to 29 ksi) gas, typically argon, to the dense surface skin of the component at a temperature below the solidus but high enough to maximize plastic flow to enhance atom/vacancy diffusion to heal the internal porosity (Ref 30, 40-42). A pore will initially shrink with plastic flow and then by diffusional

mechanisms. The goals of HIP include reduction of voids, total production costs, property scatter, improved reliability, and extended service life. The thermomechanical process collapses the gas-filled internal pores when the equilibrium pressure of the entrapped gas equals the applied pressure. The ideal pore shape is spherical to ensure isostatic pressure has been applied to the entire pore region. In some cases, however, subsequent heat treatments result in pore regrowth (Ref 43). Insoluble gases such as argon, nitrogen, and helium are often used in the processing environments for metal components.

There are four main mechanisms by which pores are eliminated by HIP: plastic flow, power-law creep, Coble (grain-boundary) creep, and Nabarro–Herring (lattice) creep (Ref 30). In sum, all mechanisms eventually lead to a densified component; however, the rate at which the pores are eliminated varies according to the mechanism selected. Plastic flow tends to vary as a function of pore fraction, where pore fraction and flow stress resemble an inverse relationship. Pores shrink as hydrostatic pressure exceeds the reduced yield point of the material at the HIP temperature, allowing for local plastic flow on the microscopic scale (Ref 40). The power-law creep mechanism alternatively uses diffusion and a transfer of atoms and vacancies to and from pinned dislocations that can be used to climb around the obstacle and through the lattice. The Coble and Nabarro–Herring creep mechanisms are diffusion processes that take place at the slowest rates and thus primarily at the latter stages of densification. Surface energy is the primary driving force associated with shrinkage via diffusion. Movement of atoms to the pore surface and vacancies from the pore surface into the bulk cease the final stages of densification. Coble creep transitions the atom/vacancy movement via grain boundaries, while Nabarro–Herring creep diffuses this atom/vacancy movement within the lattices (Ref 30, 40). Materials that are creep resistant do not have the capabilities to perform pore removal based on the latter mechanisms (Ref 41).

3.3 Sensing Technologies

Metal AM processing lacks robustness due to the complexity encompassing the AM process and the susceptibility of the process to form property-degrading defects. Efforts to detect defects using x-ray computed tomography and to heal the pores through postprocessing HIP have shown significant improvements to the as-built structural integrity of AM components. Nonetheless, metal AM postprocessing and inspection are both cost- and time-expensive, restricting the widespread use of AM for critical components. Thus, in situ methods for sensing defects derived from ex situ inspection techniques have recently been integrated into PBF and DED processes to conserve money and time spent postprocessing.

Several investigations have highlighted the potential for using a variety of noncontact thermal, optical, and ultrasound techniques as an appropriate means for inspecting AM components. Thermal and optical techniques have been more widely integrated than their counterpart—ultrasonics—due to their user-friendly interfaces, limited effects from surface roughness, and reduction in data processing of collected results. Conversely, ultrasonic investigations have viewed these as challenges to overcome. The potential for each of these nondestructive evaluation (NDE) methods (thermal, optical, and ultrasonic) is apparent for the evaluation of AM metal alloys; therefore, extended opportunities for growth continue to be sought.

3.4 Thermal Process-Monitoring Methods

Thermal techniques collect temperature profiles from irradiated surfaces to help predict areas with less fusion, where defects are likely to be present. Thermal NDE techniques, including infrared thermography and pyrometry, have sought integration in both PBF and DED chambers and collected temperature gradients during the deposition process (Ref 44-52). Infrared cameras provided high spatial and temporal information of two-dimensional surface areas for PBF (Ref 47, 50), while energy measurements were assessed for DED processes (Ref 53). Alternatively, discrete temperature measurements were collected by using pyrometry, and the data points collected were used to evaluate changes in thermal profiles with alterations in the powder feed rates and power in the DED process (Ref 45, 48, 51). Thermal measurements continue to lack valuable subsurface defect and thermal evolution information due to the limited depth of inspection for either AM process (Ref 47, 50, 54). Uncertainties in emissivity, motion blur, and reflection measurements have contributed to unreliable and misinterpreted information (Ref 49, 50, 55). Nevertheless, thermal techniques such as pyrometry have been coupled with high-speed cameras to monitor the build process (Ref 45, 48, 51, 56-58). Solidification and thermal histories of the entire build may be described by monitoring the irradiance of the layer-by-layer process (Ref 44-52).

3.5 Optical Process-Monitoring Methods

Optical measurement devices, such as high-speed cameras that use charge-coupled devices, complementary metal oxide semiconductor detectors, and optical emission spectroscopy (OES), have previously been integrated for monitoring in situ processes (Ref 11, 53, 56-59). Optical techniques are often used to collect information about the surface of a build layer, such as surface roughness, defects that may be caused by a damaged recoater blade, regions of buildup, or unmelted powder. These devices, based on light collection, are capable of monitoring the evolution of the melt pool, although their detection capability does not provide information about internal geometries that may develop during the build process (Ref 57, 58). The wide availability and inexpensiveness of high-speed cameras operable in the near-infrared regime make optical techniques an easy, affordable integration device for inspection. A technique such as OES has long been used to understand the physical mechanisms and monitoring conditions during laser material processing (Ref 7), including measuring excitation temperatures of iron, chromium, and magnesium vapors that corresponded to welding defects (Ref 60). Most recently, OES has been adopted into AM processes to identify lack-of-fusion defects within builds while also showing potential for implementing emission signals from plasma plumes for identifying hardness, surface appearance, clad dilution, and microstructures (Ref 7, 61, 62). Optical techniques have successfully captured surface features for each layer during the build, although methods continue to face image-processing challenges related to capture time and resolution (Ref 11, 53, 56-59). One of the main challenges to using optical techniques for an in situ inspection method is the inability of the process to achieve an adequate speed required for closed-loop feedback (Ref 57-59, 63).

3.6 Ultrasonic Process-Monitoring Methods

Ultrasonic techniques include both contact and noncontact methods for generating pulsed waves through a material, where the mechanical energy is either absorbed or reflected, then detected by a receiver, and transformed into electronic signals (Ref 64). Detected signals include extensive subsurface feature and surface information (Ref 9, 65-67). Variation in signal information may be due, in part, to differences in density and geometry that have pointed to defects in structural components (Ref 62, 68-70). Previous ultrasonic investigations have revealed elastic properties, grain size, texturing, and phase-change information for unique metal alloys through modeling and empirical methods (Ref 71-78).

Complexities exclusive to each AM process have dictated the feasibility of integrating either contact or noncontact tools for in situ monitoring. In an ex situ case, either may be used to provide subsurface or surface details. However, immediate correction of discovered defects is not possible. The PBF processes have implemented contact piezoelectric transducers for subsurface flaw identification in components based on the analysis of wave velocity variability (Ref 79). However, deposition of additional layers skewed the wave velocity measurements. Results suggested a degree of unreliability in measurements for multilayer components (Ref 79). Noncontact techniques, on the other hand, have not been widely adapted as an in situ monitoring technique due to the complexity involved in signal processing and detection alignment with the build process. Preliminary investigations using noncontact techniques, such as spatially resolved microscopy (Ref 67), laser ultrasonics (Ref 9, 80), and acoustic emission testing (Ref 70), have shown great promise for investigating AM materials on an ex situ level. Ultrasonic characterization and inspection offers additional bulk material property and subsurface information of internal geometries not available in alternate inspection techniques, although the complexity of the signal information is not easily interpretable (Ref 81, 82). Thus, ultrasonic techniques suggest continuing advancement for the evaluation of AM metal processes.

3.7 Design Strategies

Metal AM parameter development often cycles through a series of steps to obtain more information about how new alloys respond to different process parameters. These parameters are based on a set of conditions that have been previously implemented for other alloys. While in most cases it is ideal to produce structures without porosity, during the parameter-development stages and especially when trying to implement a new instrument for detection, it is important to try to create consistent defect formation in builds. Previous investigations in the in situ sensing community have varied process parameters, such as hatch spacing, powder flow, heat input, slicing strategies, intentional hollow structures in the computer-aided design (CAD) model, and so on, to understand what parameter or combination of parameters influenced the consistent formation of defects. The listed parameters effectively change the percent overlap of adjacent tracks, mass flow into a molten pool, amount and time an alloy is subjected to heat, and internal design of the structure. Researchers investigating in situ sensing techniques create consistent defects to verify their novel technique by using the current qualifying ex situ techniques for detecting defects, the novel technique ex situ, followed by establishing the validity of the novel technique in situ. Furthermore, applications that require porous structures, particularly those desirable for metallic foams or medical applications, must implement CAD and process parameter design to achieve consistent results.

4. Current Knowledge Gap

Metal AM has captured the attention of industry and researchers alike, both of whom are seeking to take advantage of the design opportunities and unique alloy features offered by this process. However, while the novel advancements present improved properties and intricate design features, complexities of the AM process continue to present consistent challenges that have yet to be resolved.

Fusion-based defects continue to be a recurring problem with AM components. While most defects can be detected by nondestructive inspection techniques and relieved by postprocessing HIP, consistency has yet to be achieved for processing the same alloy for multiple processing chambers. Defects that are unable to be relieved based on their size or their connectedness to the surface of the component are subjected to being scrapped. Thus, an understanding of the types of defects formed in each process, their mechanism of formation, the processing parameters that influence their formation, and the types of impurities to avoid during processing has the potential to improve the robustness of AM for processing.

References

1. T. DebRoy, H.L. Wei, J.S. Zuback, T. Mukherjee, J.W. Elmer, J.O. Milewski, A.M. Beese, A. Wilson-Heid, A. De and W. Zhang, Additive Manufacturing of Metallic Components Process Structure and Properties, *Prog. Mater. Sci.*, 2018, **92**(Suppl. C), p 112–224. https://doi.org/10.1016/j.pmatsci.2017.10.001
2. W.J. Sames, F.A. List, S. Pannala, R.R. Dehoff and S.S. Babu, The Metallurgy and Processing Science of Metal Additive Manufacturing, *Int. Mater. Rev.*, 2016, **6**(5), p 315–360. https://doi.org/10.1080/09506608.2015.1116649
3. M. Gorelik, Additive Manufacturing in the Context of Structural Integrity, *Int. J. Fatigue*, 2017, **94**, p 168–177. https://doi.org/10.1016/j.ijfatigue.2016.07.005
4. J.C. Lippold, *Welding Metallurgy and Weldability*, Wiley, Hoboken, 2015, p 1–400. https://doi.org/10.1002/9781118960332
5. M. Khanzadeh, S. Chowdhury, M.A. Tschopp, H.R. Doude, M. Marufuzzaman and L. Bian, In-situ Monitoring of Melt Pool Images for Porosity Prediction in Directed Energy Deposition Processes, *IISE Trans.*, 2019, **51**(5), p 437–455. https://doi.org/10.1080/24725854.2017.1417656
6. T. Vilaro, C. Colin and J.D. Bartout, As-Fabricated and Heat-Treated Microstructures of the Ti-6A1-4V Alloy Processed by Selective Laser Melting, *Metall Mater. Trans. A Phys. Metall. Mater. Sci.*, 2011, **42**(10), p 3190–3199. https://doi.org/10.1007/s11661-011-0731-y
7. A. Nassar, T. Spurgeon, and E. Reutzel, "*Sensing Defects during Directed-Energy Additive Manufacturing of Metal Parts Using Optical Emissions Spectroscopy*," Solid Freeform Fabrication Symposium (SFF) (Austin, TX), Aug 2014
8. D. Cerniglia, M. Scafidi, A. Pantano and J. Rudlin, Inspection of Additive-Manufactured Layered Components, *Ultrasonics*, 2015, **62**, p 292–298. https://doi.org/10.1016/j.ultras.2015.06.001
9. S. Everton, P. Dickens, C. Tuck and B. Dutton, Using Laser Ultrasound to Detect Subsurface Defects in Metal Laser Powder Bed Fusion Components, *JOM*, 2018, **70**(3), p 378–383. https://doi.org/10.1007/s11837-017-2661-7

10. S.K. Everton, M. Hirsch, P. Stravroulakis, R.K. Leach and A.T. Clare, Review of in-situ Process Monitoring and in-situ Metrology for Metal Additive Manufacturing, *Mater. Des.*, 2016, **95**, p 431–445. https://doi.org/10.1016/j.matdes.2016.01.099
11. E.W. Reutzel and A.R. Nassar, A Survey of Sensing and Control Systems for Machine and Process Monitoring of Directed-Energy, Metal-Based Additive Manufacturing, *Rapid Prototyp. J.*, 2015, **21**(2), p 159–167. https://doi.org/10.1108/RPJ-12-2014-0177
12. V. Manvatkar, A. De and T. Debroy, Heat Transfer and Material Flow During Laser Assisted Multi-Layer Additive Manufacturing, *J. Appl. Phys.*, 2014, **116**(12), p 124905. https://doi.org/10.1063/1.4896751
13. J.J. Blecher, T.A. Palmer and T. Debroy, Porosity in Thick Section Alloy 690 Welds—Experiments, Modeling, Mechanism, and Remedy, *Weld. J.*, 2016, **95**(1), p 17s–26s
14. A. Matsunawa, J.D. Kim, N. Seto, M. Mizutani and S. Katayama, Dynamics of Keyhole and Molten Pool in Laser Welding, *J. Laser Appl.*, 1998, **10**(6), p 247–254. https://doi.org/10.2351/1.521858
15. S. Katayama, Y. Kobayashi, M. Mizutani and A. Matsunawa, Effect of Vacuum on Penetration and Defects in Laser Welding, *J. Laser Appl.*, 2001, **13**(5), p 187–192. https://doi.org/10.2351/1.1404413
16. Y. Kawahito, M. Mizutani and S. Katayama, Elucidation of High-Power Fibre Laser Welding Phenomena of Stainless Steel and Effect of Factors on Weld Geometry, *J. Phys. D Appl. Phys.*, 2007, **40**(19), p 5854–5859. https://doi.org/10.1088/0022-3727/40/19/009
17. H. Zhao and T. DebRoy, Macroporosity Free Aluminum Alloy Weldments Through Numerical Simulation of Keyhole Mode Laser Welding, *J. Appl. Phys.*, 2003, **93**(12), p 10089–10096. https://doi.org/10.1063/1.1573732
18. S.A. Khairallah, A.T. Anderson, A. Rubenchik and W.E. King, Laser Powder-Bed Fusion Additive Manufacturing: Physics of Complex Melt Flow and Formation Mechanisms of Pores Spatter Denudation Zones, *Acta Mater.*, 2016, **108**, p 36–45. https://doi.org/10.1016/j.actamat.2016.02.014
19. C. Zhao, K. Fezzaa, R.W. Cunningham, H.D. Wen, F. De. Carlo, L.Y. Chen, A.D. Rollett and T. Sun, Real-Time Monitoring of Laser Powder Bed Fusion Process Using High-Speed X-Ray Imaging and Diffraction, *Sci. Rep.*, 2017 https://doi.org/10.1038/s41598-017-03761-2
20. R.E. Trevisan, D.D. Schwemmer, and D.L. Olson, Chap. 3, The Fundamentals of Weld Metal Pore Formation, *Materials Processing: Theory and Practices*, D.L. Olson, R. Dixon, and A.L. Liby, Ed., Elsevier Science Publishers, 1990, p 79–115. https://doi.org/10.1016/B978-0-444-87427-6.50009-5
21. H. Fredriksson and I. Svensson, Mechanism of Pore Formation in Metals, *Metall Trans. B Process Metall.*, 1976, **7**(4), p 599–606. https://doi.org/10.1007/BF02698593
22. H. Taheri, M.M. Shoaib, L.W. Koester, T.A. Bigelow, P.C. Collins and L.J. Bond, Powder Based Additive Manufacturing—a Review of Types of Defects, Generation Mechanisms, Detection, Property Evaluation and Metrology, *Int. J. Addit. Subtrac. Mater. Manuf.*, 2017, **1**(2), p 172–209. https://doi.org/10.1504/IJASMM.2017.10009247
23. C.E. Cross, *On the Origin of Weld Solidification Cracking Hot Cracking Phenomena in Welds*, Springer, New York, 2005, p 3–18
24. J.N. Dupont, C.V. Robino and A.R. Marder, Solidification and Weldability of Nb-Bearing Superalloys, *Weld. J.*, 1998, **77**(10), p 417s–431s. https://doi.org/10.2172/515586
25. W. Pellini, Strain Theory of Hot Tearing, *Foundry*, 1952, **80**(11), p 125–133
26. T. Senda, F. Matsuda and G. Takano, Solidification Crack Susceptibility for Weld Metals with the Trans-Varestraint Test, Part 2: commercially used Aluminum and Aluminum Alloys, *Yosetsu Gakkai-Shi*, 1973, **42**(1), p 48–56. https://doi.org/10.2207/qjjws1943.42.48
27. S. Shiva, I.A. Palani, S.K. Mishra, C.P. Paul and L.M. Kukreja, Investigations on the Influence of Composition in the Development of Ni-Ti Shape Memory Alloy Using Laser Based Additive Manufacturing, *Opt. Laser Technol.*, 2015, **69**, p 44–51. https://doi.org/10.1016/j.optlastec.2014.12.014
28. G.P. Dinda, L. Song and J. Mazumder, Fabrication of Ti6Al-4V Scaffolds by Direct Metal Deposition, *Metall. Mater. Trans. A, Phys. Metall. Mater. Sci.*, 2008, **39**(12), p 2914–2922. https://doi.org/10.1007/s11661-008-9634-y
29. A.V. Gusarov, M. Pavlov, and I. Smurov, Residual Stresses at Laser Surface Remelting and Additive Manufacturing, Lasers in Manufacturing 2011: Proceedings of the Sixth International WLT Conference on Lasers in Manufacturing, Vol 12, Part A, p 248–254. (2011). https://doi.org/10.1016/j.phpro.2011.03.032
30. V. Samarov and V. Goloveshkin, Modeling of Hot Isostatic Pressing, *Metals Process Simulation,* Vol 22B, *ASM Handbook,* D.U. Furrer and S.L. Semiatin, Ed., ASM International, 2010, p 335–342. https://doi.org/10.31399/asm.hb.v22b.a0005509
31. S.L. Kang, Part II: Solid State Sintering Models and Densification, Sintering: Densification, Grain Growth and Microstructure, Elsevier Butterworth-Heinemann, Burlington, MA, 2005
32. R.L. Coble, Sintering of Crystalline Solids, Part I: Intermediate and Final State Diffusion Models, *J. Appl. Phys.*, 1961, **32**, p 789–792. https://doi.org/10.1063/1.1736107
33. R.L. Coble and J.E. Burke, Sintering in Ceramics, *Progress in Ceramic Science*. J.E. Burke Ed., Pergamon Press, New York, 1963, p 197–252
34. I.M. Robertson and G.B. Schaffer, Review of Densification of Titanium Based Powder Systems in Press and Sinter Processing, *Powder Metall.*, 2010, **53**(2), p 146–162. https://doi.org/10.1179/174329009X434293
35. S.A. Matar, M.J. Edirisinghe, J.R.G. Evans and E.H. Twizell, Diffusion of Degradation Products in Ceramic Moldings during Pyrolysis: Effect of Geometry, *J. Am. Ceram. Soc.*, 1996, **79**(3), p 749–755. https://doi.org/10.1111/j.1151-2916.1996.tb07938.x
36. P.K. Lu and J.J. Lannutti, Effect of Density Gradients on Dimensional Tolerance during Binder Removal, *J. Am. Ceram. Soc.*, 2000, **83**(10), p 2536–2542. https://doi.org/10.1111/j.1151-2916.2000.tb01587.x
37. H.H. Angermann and O. Vanderbiest, Scientific and Technological Progress in Binder Burnout from Metal Injection-Molded Compacts, *Mater. Manuf. Process.*, 1995, **10**(3), p 439–451. https://doi.org/10.1080/10426919508935037
38. N. Kumbhar and A. Mulay, Post Processing Methods Used to Improve Surface Finish of Products Which are Manufactured by Additive Manufacturing Technologies: a Review, *J. Inst. Eng. (India) C.*, 2018, **99**(4), p 481–487
39. A.R. Marder (1997) Effects of Surface Treatments on Materials Performance, *Materials Selection and Design*, G.E. Dieter, Ed., ASM International, 1997, p 470–490. https://doi.org/10.31399/asm.hb.v20.a0002466
40. H.V. Atkinson and S. Davies, Fundamental Aspects of Hot Isostatic Pressing: an Overview, *Metall. Mater. Trans A Phys. Metall. Mater. Sci.*, 2000, **31**(12), p 2981–3000
41. S.J. Mashl (2015) Powder Metallurgy Processing by Hot Isostatic Pressing. In: P. Samal and J. Newkirk, Ed., Powder Metallurgy. p 260–270
42. S.J. Mashl, *Hot Isostatic Pressing of Castings, Casting*, Vol 15 ASM International, USA, 2008, p 408–416
43. S. Tammas-Williams, R.I. Withers, I. Todd and P.B. Prangnell, Porosity Regrowth during Heat Treatment of Hot Isostatically Pressed Additively Manufactured Titanium Components, *Scr. Mater.*, 2016, **122**, p 72–76. https://doi.org/10.1016/j.scriptamat.2016.05.002
44. D.M. Hu and R. Kovacevic, Sensing, Modeling and Control for Laser-Based Additive Manufacturing, *Int. J. Mach. Tools Manuf.*, 2003, **43**(1), p 51–60. https://doi.org/10.1016/S0890-6955(02)00163-3
45. T. Hua, C. Jing, L. Xin, F.Y. Zhang and W.D. Huang, Research on Molten Pool Temperature in the Process of Laser Rapid Forming, *J. Mater. Process. Technol.*, 2008, **198**(1–3), p 454–462. https://doi.org/10.1016/j.jmatprotec.2007.06.090
46. M. Islam, T. Purtonen, H. Piili, A. Salminen and O. Nyrhila, Temperature Profile and Imaging Analysis of Laser Additive Manufacturing of Stainless Steel, *Lasers Manuf.*, 2013, **41**, p 828–835. https://doi.org/10.1016/j.phpro.2013.03.156
47. H. Krauss, C. Eschey, and M. Zaeh, *Thermography for Monitoring the Selective Laser Melting Process*, Proceedings of the Solid Freeform Fabrication Symposium, 2012
48. L. Wang, S.D. Felicelli, and J.E. Craig, "*Thermal Modeling and Experimental Validation in the LENS Process*," 18th Solid Freeform Fabrication Symposium (Austin, TX), 2007
49. B. Lane, E. Whitenton, V. Madhavan and A. Donmez, Uncertainty of Temperature Measurements by Infrared Thermography for Metal Cutting Applications, *Metrologia*, 2013, **50**(6), p 637–653. https://doi.org/10.1088/0026-1394/50/6/637
50. S. Moylan, E. Whitenton, B. Lane, and J. Slotwinski, *Infrared Thermography for Laser-Based Powder Bed Fusion Additive Manufacturing Processes*, AIP Conference Proceedings, American Institute of Physics, 2014. https://doi.org/10.1063/1.4864956

51. A.R. Nassar, J.S. Keist, E.W. Reutzel and T.J. Spurgeon, Intra-Layer Closed-Loop Control of Build Plan during Directed Energy Additive Manufacturing of Ti-6Al-4V, *Add. Manuf.*, 2015, **6**, p 39–52. https://doi.org/10.1016/j.addma.2015.03.005
52. M. Pavlov, M. Doubenskaia, and I. Smurov, *Pyrometric Analysis of Thermal Processes in SLM Technology*, Laser Assisted Net Shape Engineering 6, Proceedings of the LANE 2010, Part 2, Vol 5, 2010, p 523–531. https://doi.org/10.1016/j.phpro.2010.08.080
53. S. Karnati, N. Matta, T. Sparks, and F. Liou, *Vision-Based Process Monitoring for Laser Metal Deposition Processes*, Proceedings of the Solid Freeform Fabrication Symposium, 2013
54. J.A. Slotwinski, E.J. Garboczi and K.M. Hebenstreit, Porosity Measurements and Analysis for Metal Additive Manufacturing Process Control, *J. Res. Natl. Inst. Stand. Technol.*, 2014, **119**, p 494–528. https://doi.org/10.6028/jres.119.019
55. E.P. Whitenton, An Introduction for Machining Researchers to Measurement Uncertainty Sources in Thermal Images of Metal Cutting, *Int. J. Mach. Machinabil. Mater.*, 2012, **12**(3), p 195–214. https://doi.org/10.1504/IJMMM.2012.049255
56. S. Barua, F. Liou, J. Newkirk and T. Sparks, Vision-Based Defect Detection in Laser Metal Deposition Process, *Rapid Prototyp. J.*, 2014, **20**(1), p 77–86. https://doi.org/10.1108/RPJ-04-2012-0036
57. S. Clijsters, T. Craeghs, S. Buls, K. Kempen and J.P. Kruth, In Situ Quality Control of the Selective Laser Melting Process Using a High-Speed, Real-Time Melt Pool Monitoring System, *Int. J. Adv. Manuf. Technol.*, 2014, **75**(5–8), p 1089–1101. https://doi.org/10.1007/s00170-014-6214-8
58. T. Craeghs, S. Clijsters, E. Yasa, and J.P. Kruth, *Online Quality Control of Selective Laser Melting*, Proceedings of the Solid Freeform Fabrication Symposium (Austin, TX), 2011
59. S. Kleszczynski, J. Zur Jacobsmühlen, J. Sehrt, and G. Witt, *Error Detection in Laser Beam Melting Systems by High Resolution Imaging*, Proceedings of the Solid Freeform Fabrication Symposium, 2012
60. A. Ancona, V. Spagnolo, P.M. Lugara and M. Ferrara, Optical Sensor for Real-Time Monitoring of CO_2 Laser Welding Process, *Appl. Optics*, 2001, **40**(33), p 6019–6025. https://doi.org/10.1364/AO.40.006019
61. K. Bartkowiak, *Direct Laser Deposition Process within Spectrographic Analysis In Situ*, Laser Assisted Net Shape Engineering 6, Proceedings of the LANE 2010, Part 2, Vol 5, 2010, p 623–629. https://doi.org/10.1016/j.phpro.2010.08.090
62. L.J. Song and J. Mazumder, Real Time Cr Measurement Using Optical Emission Spectroscopy during Direct Metal Deposition Process, *IEEE Sensors J.*, 2012, **12**(5), p 958–964. https://doi.org/10.1109/JSEN.2011.2162316
63. S. Berumen, F. Bechmann, S. Lindner, J.P. Kruth, and T. Craeghs, *Quality Control of Laser- and Powder Bed-Based Additive Manufacturing (AM) Technologies*, Laser Assisted Net Shape Engineering 6, Proceedings of the LANE 2010, Part 2, Vol 5, 2010, p 617–622. https://doi.org/10.1016/j.phpro.2010.08.089
64. D.K. Pandey and S. Pandey (2010), Ultrasonics: A Technique of Material Characterization, *Acoustic Waves.* p 397–430
65. H. Cho, S. Ogawa and M. Takemoto, Non-Contact Laser Ultrasonics for Detecting Subsurface Lateral Defects, *NDTE Int.*, 1996, **29**(5), p 301–306. https://doi.org/10.1016/S0963-8695(96)00033-3
66. H. Gong, K. Rafi, H. Gu, T. Starr and B. Stucker, Analysis of Defect Generation in Ti-6Al-4V Parts Made Using Powder Bed Fusion Additive Manufacturing Processes, *Add. Manuf.*, 2014, **1–4**, p 87–98. https://doi.org/10.1016/j.addma.2014.08.002
67. R.J. Smith, M. Hirsch, R. Patel, W.Q. Li, A.T. Clare and S.D. Sharples, Spatially Resolved Acoustic Spectroscopy for Selective Laser Melting, *J. Mater. Process. Technol.*, 2016, **236**, p 93–102. https://doi.org/10.1016/j.jmatprotec.2016.05.005
68. L. Chehami, E. Moulin, J. Rosnyde, C. Prada, E. Chatelet, G. Lacerra, K. Gryllias and F. Massi, Nonlinear Secondary Noise Sources for Passive Defect Detection Using Ultrasound Sensors, *J. Sound Vib.*, 2017, **386**, p 283–294. https://doi.org/10.1016/j.jsv.2016.10.006
69. T. Tanaka and Y. Izawa, *Nondestructive Detection of Small Internal Defects in Carbon Steel by Laser Ultrasonics*, Jpn. J. Appl. Phys., 2001. https://doi.org/10.1143/JJAP.40.1477
70. F. Wang, H. Mao, D. Zhang, X. Zhao and Y. Shen, Online Study of Cracks during Laser Cladding Process Based on Acoustic Emission Technique and Finite Element Analysis, *Appl. Surf. Sci.*, 2008, **255**(5), p 3267–3275. https://doi.org/10.1016/j.apsusc.2008.09.039
71. A.P. Arguelles and J.A. Turner, Ultrasonic Attenuation of Polycrystalline Materials with a Distribution of Grain Sizes, *J. Acoust. Soc. Am.*, 2017, **141**(6), p 4347–4353. https://doi.org/10.1121/1.4984290
72. M.P. Blodgett and D. Eylon, The Influence of Texture and Phase Distortion on Ultrasonic Attenuation in Ti-6Al-4V, *J. Nondestr. Eval.*, 2001, **20**(1), p 1–16
73. T. Garcin, J.H. Schmitt, and M. Militzer, "*Application of Laser Ultrasonics to Monitor Microstructure Evolution in Inconel 718 Superalloy*," Eurosuperalloys 2014—Second European Symposium on Superalloys and Their Applications, 201410.1051/matecconf/20141407001
74. T. Garcin, J.H. Schmitt and M. Militzer, In-Situ Laser Ultrasonic Grain Size Measurement in Superalloy Inconel 718, *J. Alloy. Compd.*, 2016, **670**, p 329–336. https://doi.org/10.1016/j.jallcom.2016.01.222
75. X.B. Li, X. Han, A.P. Arguelles, Y. Song and H. Hu, Evaluating Grain Size in Polycrystals with Rough Surfaces by Corrected Ultrasonic Attenuation, *Ultrasonics*, 2017, **78**, p 23–29. https://doi.org/10.1016/j.ultras.2017.02.018
76. O.I. Lobkis and S.I. Rokhlin, Characterization of Polycrystals with Elongated Duplex Microstructure by Inversion of Ultrasonic Backscattering Data, *Appl. Phys. Lett.*, 2010 https://doi.org/10.1063/1.3416910
77. A. Shinbine, T. Garcin and C. Sinclair, In-Situ Laser Ultrasonic Measurement of the hcp to bcc Transformation in Commercially Pure Titanium, *Mater. Charact.*, 2016, **117**, p 57–64. https://doi.org/10.1016/j.matchar.2016.04.018
78. H.L. Wei, J.W. Elmer and T. DebRoy, Origin of Grain Orientation During Solidification of an Aluminum Alloy, *Acta Mater.*, 2016, **115**, p 123–131. https://doi.org/10.1016/j.actamat.2016.05.057
79. H. Rieder, A. Dillhöfer, M. Spies, J. Bamberg, and T. Hess, "*Online Monitoring of Additive Manufacturing Processes Using Ultrasound*," Eleventh European Conference on Non-Destructive Testing (ECNDT) (Prague, Czech Republic), Oct 2014. https://doi.org/10.1063/1.4914609
80. M. Klein and J. Sears, "Laser Ultrasonic Inspection of Laser Cladded 316LSS and Ti-6-4", International Congress on Applications of Lasers and Electro-Optics, *Laser Inst. Am.*, 2004. https://doi.org/10.2351/1.5060183
81. R.J. Dewhurst, D.A. Hutchins, S.B. Palmer and C.B. Scruby, Quantitative Measurements of Laser-Generated Acoustic Waveforms, *J. Appl. Phys.*, 1982, **53**(6), p 4064–4071. https://doi.org/10.1063/1.331270
82. L. Drain and C.B. Scruby, *Laser Ultrasonics Techniques and Applications*, 1st ed. Routledge, New York, 1990